ACSNANO
www.acsnano.org
ARTICLE

Study of Heat Transfer Dynamics from Gold Nanorods to the Environment *via* Time-Resolved Infrared Spectroscopy

Son C. Nguyen,[†,∥] Qiao Zhang,[†] Karthish Manthiram,[‡] Xingchen Ye,[†] Justin P. Lomont,[†] Charles B. Harris,[*,†] Horst Weller,[*,∥,○] and A. Paul Alivisatos[*,†,§,⊥,▽]

[†]Department of Chemistry, [‡]Department of Chemical and Biomolecular Engineering, and [§]Kavli Energy Nanosciences Institute, University of California, Berkeley, California 94720, United States

[⊥]Materials Sciences Division, Lawrence Berkeley National Laboratory, Berkeley, California 94720, United States

[∥]Institute of Physical Chemistry, University of Hamburg, Grindelallee 117, 20146 Hamburg, Germany

[▽]The Hamburg Centre for Ultrafast Imaging, University of Hamburg, Luruper Chaussee 149, 22761 Hamburg, Germany

[○]Department of Chemistry, Faculty of Science, King Abdulaziz University, Jeddah 21589, Saudi Arabia

Supporting Information

ABSTRACT: **Studying the local solvent surrounding nanoparticles is important to understanding the energy exchange dynamics between the particles and their environment, and there is a need for spectroscopic methods that can dynamically probe the solvent region that is in nearby contact with the nanoparticles. In this work, we demonstrate the use of time-resolved infrared spectroscopy to track changes in a vibrational mode of local water on the time scale of hundreds of picoseconds, revealing the dynamics of heat transfer from gold nanorods to the local water environment. We applied this probe to a prototypical plasmonic photothermal system consisting of organic CTAB bilayer capped gold nanorods, as well as gold nanorods coated with varying thicknesses of inorganic mesoporous-silica. The heat transfer time constant of CTAB capped gold nanorods is about 350 ps and becomes faster with higher laser excitation power, eventually generating bubbles due to superheating in the local solvent. Silica coating of the nanorods slows down the heat transfer and suppresses the formation of superheated bubbles.**

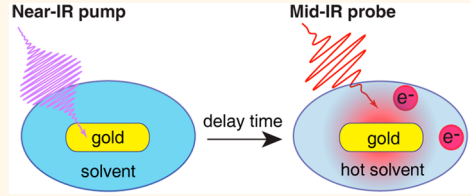

KEYWORDS: *plasmonic nanoparticle, silica coating, heat transfer, electron ejection, time-resolved infrared spectroscopy*

Heat transfer from plasmonic nanoparticles (NPs) to the environment is a fundamental process with many potential and emerging applications, such as photothermal therapy,[1,2] drug delivery,[3,4] solar steam,[5] solar autoclaves,[6] and plasmon-mediated chemical reactions.[7,8] This heat transfer starts with the absorption of a photon and conversion of the photon energy to heat in the NPs. The heat is then transferred through the interface to the local environment and eventually to the bulk.[9] In the potential applications mentioned above, the elevation of the temperature above a critical threshold within a volume surrounding the nanoparticle is the desired feature that determines the utility of the nanoparticles. Studying heat transfer dynamics from the NPs, through their interface, and then to the environment is therefore a key step to understand and utilize this local heat.

Plasmonic NPs of interest for delivering heat may be encapsulated in a variety of shells, both organic and inorganic,[2,4] and these coatings can play a decisive role in determining the flow of heat and the maximum temperature rise within the coatings themselves and to the nearby solvent. Thus, it is of great interest to be able to probe the heat flow in a variety of such samples. Here we establish and calibrate a transient ultrafast spectroscopic probe of the local temperature surrounding plasmonic gold NPs in water and with various surface modifications. This probe is based on changes in infrared combination absorption bands of water, which are very sensitive to temperature. Changes in infrared absorption are used to monitor the heat flow into the solvent from the NP, *via* the intervening coatings.

We have chosen a set of model systems to examine the nanoscale heat flow (Figure 1A). First, we chose to study gold nanorods (GNRs), because they are a prototypical plasmonic system for photothermal excitation. We also chose a set of systems with a typical organic coating bilayer, cetyltrimethylammonium bromide (CTAB). Organic bilayers such as CTAB are used to control the shape and size during synthesis and to

Received: October 21, 2015
Accepted: February 3, 2016
Published: February 3, 2016

© 2016 American Chemical Society

DOI: 10.1021/acsnano.5b06623
ACS Nano 2016, 10, 2144–2151

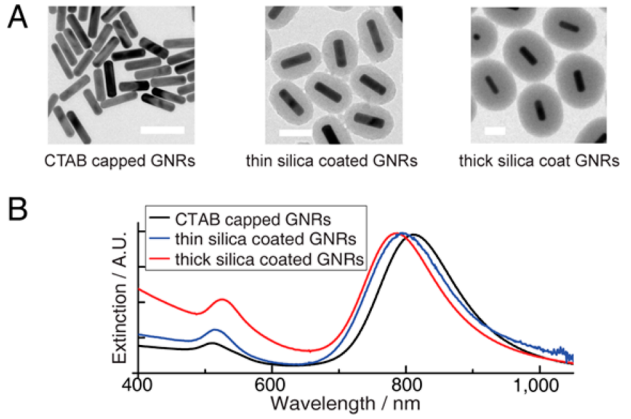

Figure 1. (A) TEM images of particles in this study, including CTAB capped GNRs and porous-silica coated GNRs. Scale bar, 100 nm. (B) UV−vis spectra of the corresponding colloidal solutions with the SPR absorption at ∼800 nm for TRIR experiment.

maintain colloidal stability of plasmonic NPs afterward. Such bilayers may be thermally insulating, and thus, it is of interest to observe the heat flow through this layer. Once we determined the effective volume nearby a CTAB capped NP that was heated, we then examined two more samples. One with a shell of porous silica that is roughly equal in volume to that which is heated when the only coating is CTAB, and one with a much larger volume. Frequently, investigators are interested in heating a sequestered layer in order to release molecules for drug delivery,[2,4] or in order to promote a chemical reaction within a confined volume near a NP.[10] These samples effectively enclose the range of heat transfer regime of most interest for such purposes. The heat flow dynamics in them can serve as a guide to the design of NP systems for a desired photothermal heating application.

Heat loss *from* the NPs to the environment has been studied previously,[11,12] but only limited prior experimental work focused on examining the flow of the heat *into* the environment surrounding the NPs.[13] Transient absorption spectroscopy has been intensively and very elegantly used to study these heat losses,[11,12,14] as it can probe the temperature drop of the NPs themselves.[15,16] The relationship however between the NP temperature decrease and the increase in optical absorption of the NPs is complex, in part because of the unknown physical state of the solvent, making it difficult so far to calibrate the heat transfer dynamics using this spectroscopic technique. Here, we provide a complement to this prior work, by measuring the time-resolved infrared (TRIR) spectra of the solvent. We exploit the high sensitivity of the solvent IR spectrum to heat transfer,[17] and demonstrate that this spectroscopic method is sensitive enough to detect the physical state of the local solvent in the ultrafast regime.

RESULTS AND DISCUSSION

Calibration of the IR Spectrum as a Thermometer Using Steady-State Heating. The IR absorption response of water solvent in CTAB capped GNRs and silica coated GNR colloids to elevated steady-state temperatures provides essential information for calibrating the heat transfer dynamics in the TRIR experiment, as heat transfer causes increased temperatures and corresponding decreases in the relevant IR absorption of water.

For CTAB capped GNR solutions, we know that the heat diffusion length in local water on the ultrafast time scale is on the order of tens of nanometers from each GNR (*vide infra*). This distance is significantly larger than the critical distance (less than 3 nm from the surfactant[18,19]) over which water behaves differently from the bulk. Thus, we can use the steady-state response of bulk water in the colloidal solutions (Figure 2B) to interpret the sum of the ultrafast responses of the local water in the nanoscale region surrounding each individual GNR in the pump−probe experiment (Figure 3C,E). The spectra of colloidal solutions subject to steady-state heating have very similar changes in absorption bands and temperature dependencies to those of pure water (Figures 2A,B and S1A−E), confirming these bands arise from water. We investigated the combination band of the H−O−H bend and libration modes in the spectral region from 1960 to 2210 cm^{-1}. This region has an

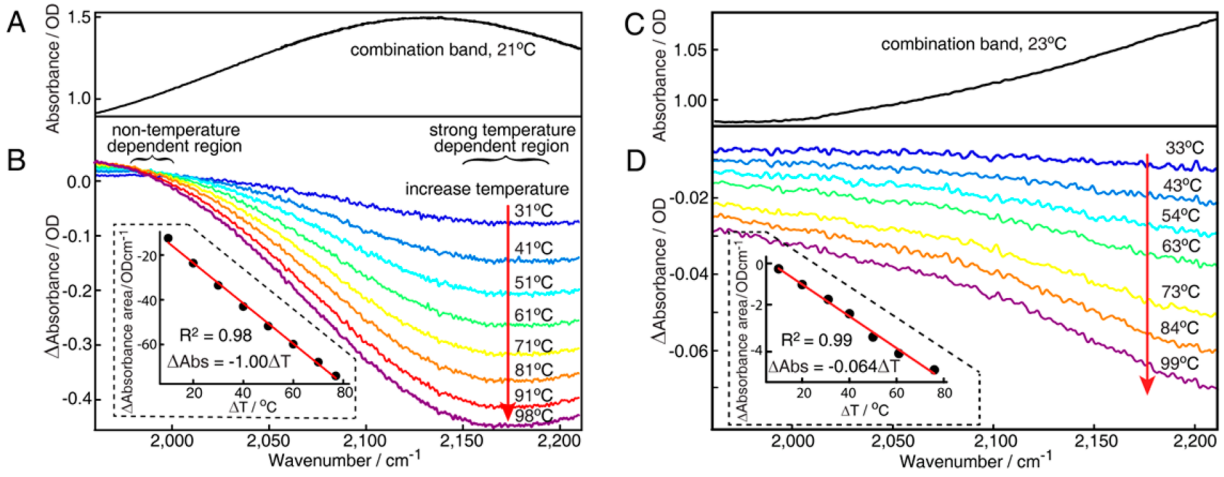

Figure 2. IR spectra of water in CTAB capped GNRs colloidal solution and a thin film of thick silica-coated GNRs. (A) Broad absorption of the combination band of water solvent in aqueous colloidal CTAB capped GNRs solution in a 70 μm spacer cell. (C) Combination band of water in a ∼200 μm thin film of thick silica-coated GNRs. The film was prepared by drop casting the colloidal solution on a CaF_2 window, drying overnight in air, then sandwiching between two CaF_2 windows during the elevated temperature measurement to prevent water evaporation. (B and D) Difference spectra in which A and C were subtracted from spectra collected at elevated temperature, respectively. The inset shows the linear dependence between temperature change and absorption area change (integrated from 2140 to 2180 cm^{-1}).

DOI: 10.1021/acsnano.5b06623
ACS Nano 2016, 10, 2144−2151

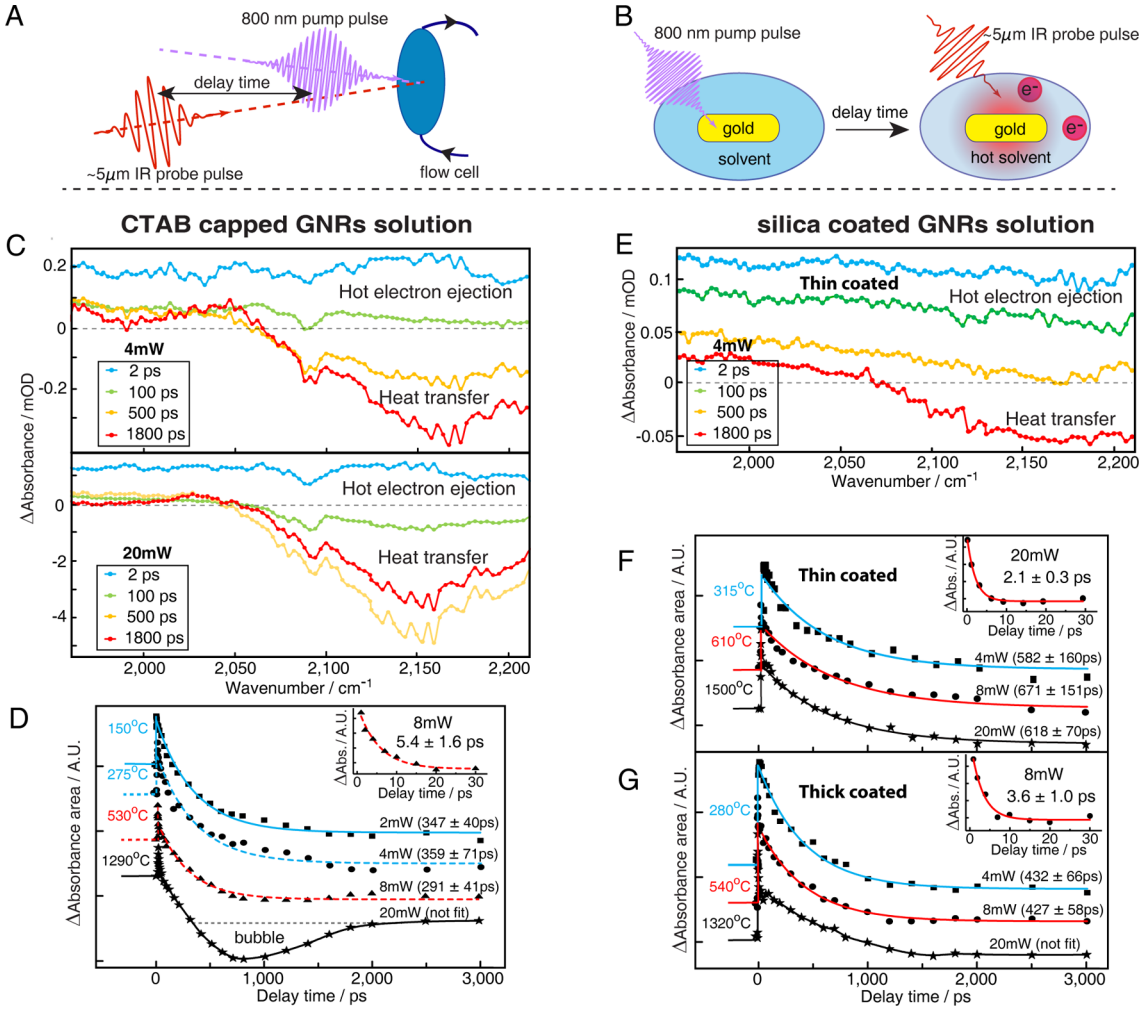

Figure 3. Scheme of the pump−probe TRIR experiment and the TRIR spectra of water in colloidal CTAB capped GNRs and silica-coated GNRs solutions. (A) Scheme of laser pulses overlapped in the region of 200 μm in a flow cell. (B) The probe TRIR signal in (A) is attributed to the sum signal of water surrounding locally each NP in the probe region. (C and E) Spectra at various excitation powers and delay times; the artifact weak absorption at 2090 cm^{-1} in C is due to the scattering of the pump pulse to the detector (Supporting Information, Section 3). (D, F, and G) Kinetic traces of the 2140−2180 cm^{-1} region of the CTAB capped, thin and thick silica-coated GNR solutions, respectively, show a first fast decay in tens of picoseconds and a later slow decay in nanoseconds. Fitting time constants (95% confidence) at later delay times (30−3000 ps) at various laser powers. The insets show representative fast decay of signals at early delay times (1−30 ps). Temperature values on the left of each kinetic trace show the estimated highest temperature (Supporting Information, Section 5) of the NPs based on the photon fluences. Kinetic traces at 20 mW in (D and G) are not possible to fit to single exponential function.

appropriate extinction coefficient to perform the TRIR experiments while the sample flows through an optical cell with 70 μm spacers, which allows us to refresh the sample after each pair of pump−probe laser shots. The absorbance in the spectral region of the fundamental bands is so high that it is infeasible to do spectroscopy of these bands in the flow cell. The absorption coefficient of the combination band is sensitive to temperature changes due to modification of the hydrogen bond network.[20] Figure 2B shows a strong temperature dependence for the IR absorption of colloidal CTAB capped GNRs in the high energy region, while the low energy region shows a smaller effect. In particular, we chose to integrate over the peak area from 2140 to 2180 cm^{-1} to quantify this dependence since this region has the strongest response, as well as a linear relationship between IR absorption change and temperature change. We also examined the nontemperature-dependent region, from 1980 to 2000 cm^{-1}, which helped us to assign the TRIR spectral feature in this region to electron solvation rather than heat transfer (*vide infra*).

For silica-coated GNR solutions, it is worth considering that the large amount of water in the mesoporous silica also has an IR absorption response to changes in temperature. To address this, an air-dried thin film of thick silica-coated GNRs was prepared, and the IR spectra were collected at elevated temperatures. The spectra show a comparable response of water in the silica shell to that in the colloidal solution (Figure 2C,D). This is expected, because the silica pores are large enough (about 4 nm in diameter[21]) that a large portion of water in the pores behave similarly to bulk water.[22] The peak area from 2140 to 2180 cm^{-1} also shows a linear temperature dependence.

Heat Transfer Dynamics of Organic CTAB Capped GNRs. The TRIR spectra after pulsed photoexcitation of the colloidal solution at the SPR absorption, shown in Figure 3C, closely resemble the different spectra at elevated steady-state temperatures in Figure 2B, indicating heat is transferred to a small volume of water surrounding each GNR on a time scale of a few hundred picoseconds. Here we focus specifically on the

DOI: 10.1021/acsnano.5b06623
ACS Nano 2016, 10, 2144−2151

dynamics on this time scale of hundreds of picoseconds. Note that there is also a transient response of the system on a time scale of a few picoseconds, about 2 orders of magnitude faster than the time scale on which heat flows out of the nanoparticles. We attribute this transient positive ΔOD signal to the vibrational modes of water during the process of solvating electrons[23,24] ejected from the GNRs, and to subsequent geminate recombination of the vast majority of these electrons with the nanoparticles. Photoinduced electron ejection to the solvent had been proposed in a previous transient absorption spectroscopic study on silver NPs.[25] However, detecting solvated electrons was impossible in that experiment due to the strong and broad absorption bands of the nanoparticles. Our TRIR spectroscopy does not suffer from this spectral interference from the nanoparticles, thus allowing us to more unambiguously probe this electron ejection. This early time electronic behavior is of great interest, and is the subject of a complementary study that is currently in preparation.

Returning to our main subject, energy transfer on the vibrational time scale of hundreds of picoseconds, we note that the increasingly negative value of ΔOD at longer delay time indicates that more heat is transferred from the GNRs to water. Due to the linear dependence between the IR absorption change and temperature rise (inset in Figure 2B), the TRIR spectra reflect the total amount of heat being transferred to water, regardless of the temperature profile of the local water. Kinetic traces of this spectral region area fit well to single exponential functions to extract the heat transfer time constants (Figure 3D). After 2 ns, the spectra show little change, indicating most of the heat is transferred. This dissipated heat is not expected to diffuse out of the micrometer-size probe area on this time scale (Supporting Information, Section 3).[17]

To evaluate the influence of initial temperature of the irradiated NPs on their heat transfer dynamics, we conducted the experiments at various excitation powers, ranging from 2 to 20 mW, equivalent to a fluence from 0.3 to 3 mJ/(cm^2·pulse) or a laser field intensity of (0.3−3) × 10^9 W/(cm^2·pulse), and the estimated initial temperatures of the NPs range from 150 to 1290 °C (Figure 3D and Supporting Information, Section 5). At 2, 4, or 8 mW, the heat transfer times are very similar (*ca.* 350 ps) within experimental error. Similar power independent behavior of heat transfer times also has been observed for spherical gold NPs with initial temperature rises on the order of 100 °C.[12] At the highest power tested, 20 mW, the kinetic trace is too linear at early delay times to fit to an exponential function, however it clearly appears that heat transfer happens faster. The results of the 20 mW experiments indicate that the heat transfer rate can be tuned to be faster when a higher excitation power is applied. We speculate that the very large temperature difference between the NPs and environment in this experiment causes faster heat transfer. We cannot eliminate another possibility that some capping ligands are transiently desorbed from the GNRs under this high excitation power, which would cause some degree of direct contact between the GNRs and water, thus supporting faster heat transfer.

We believe most of the heat transfers through the organic coating to go to the surrounding water, because the GNR surface is covered by a bilayer of CTAB, and probably some sodium oleate used for the GNR synthesis. Two pieces of evidence for the high coverage of surfactant on GNRs are that (i) the equilibrium concentration of surfactant in the spectrally studied sample is 1.6 mM (Supporting Information, Section 1), above the critical micelle concentration, and (ii) the SPR absorption of the GNR does not change after washing with water in the sample preparation process for the TRIR experiment.[11] The heat transfer rate depends strongly on how fast heat is transferred across the GNR-capping surfactant−water interfaces as well as heat diffusion into the bulk water.[13] It is also expected that particles with a higher surface area-to-volume ratio have shorter heat transfer time. Hartland and co-workers elegantly observed this behavior for the case of spherical gold NPs (citrate capped) *via* transient absorption spectroscopy[12] and the result was further supported by a classical model for heat transfer from a sphere to an infinite medium.[26] In Hartland's work, the heat transfer time of 40 nm diameter gold NPs is 270 ps. In comparison, our GNRs, which have a nearly equivalent volume (a 35 nm diameter sphere), similar surface area, and higher surface-area-to-volume ratio, exhibited larger heat transfer time constants. We think the bilayer[11] of long carbon chain CTAB ligands on our GNRs provides more thermal resistance than the short citrate ligands on the gold NPs in Hartland's study, resulting in longer heat transfer times.

To estimate the localization of the heated solvent and the temperature rise, we used the thermal conduction value of bulk water but adapted the time scale of heat transfer from the TRIR spectra. Note that the TRIR spectroscopy can only detect the total amount of heat being transferred to the solvent but cannot provide the temperature distribution.[17] Another fact is the TRIR spectra collect the sum signal from the ensemble of many local heated solvent molecules surrounding many particles in the probe area (illustrated in Figure 3A), because the high time resolution of this technique allows us to trace the local heat before hot zones between the particles merge. Thus, this technique can give us the average dynamics of an ensemble of many single particles (illustrated in Figure 3B) and the estimation of local heat is safely calculated with a single particle model. The thermal diffusivity χ of water under ambient conditions is 0.145 nm^2/ps[27] and the mean diffusion length at delay time t is $2(\chi t)^{1/2}$.[20,28] At a 2 ns delay time, when the heat transfer is almost complete, the heat is estimated to diffuse about 34 nm from the GNR, a quite localized region in comparison to the interparticle distance of about 600 nm. To estimate the average temperature rise in this localized region at this long delay time, we chose the experimental condition at low excitation power in which the thermal diffusion is not disturbed by the superheating effect (*vide infra*). The average temperature increases are about 1.5, 3, and 6 °C for the 2, 4, and 8 mW excitation powers, respectively; these values are estimated from the absorbed energy of the laser pulse and converting this energy into heat in a solvent region up to 34 nm from each GNR (Supporting Information, Section 6). About 99% of the heat is already transferred from the GNR to the solution on this time scale. It is worth noting that the larger volume and volumetric specific heat capacity (1.7 times) of local water than those of gold are the reason why the initial temperature of the GNRs is very high but the temperature rise of the GNR and local water at nanosecond delay times is quite small. This temperature profile also indicates that the heat remains localized within a nanoscale volume for nanoseconds. In the microsecond regime, the heat diffuses to the microscale region and the temperature increase is virtually zero.

Understanding the heat transfer dynamics of NPs will help to maximize their performance in photothermal applications, because the localization of the heat and magnitude of the

DOI: 10.1021/acsnano.5b06623
ACS Nano 2016, 10, 2144−2151

temperature rise can be predicted and adjusted. The heat localization and the temperature rise of the environment surrounding the NPs depends on three factors: (i) the rate and (ii) the amount of the heat being transferred from the NPs to the local solvent, as well as (iii) the heat diffusion from the local solvent to the bulk. Since the last factor is fixed for a specific environment, the other two factors can be tuned when using excitation laser pulses with longer duration and various powers. When the duration of the excitation pulse is longer than the heat transfer time constant, the overall heat transfer time to the solvent is extended as the result of the convolution of the pulse duration and the intrinsic heat transfer time constant. Thus, the effected local heating region is expanded (see examples for 1 and 10 ns pulse in Figure S4). Increasing the power of the excitation laser will result in a linear increase in the temperature rise. Overall, balancing of these factors will give a desirable temperature profile for each application.

Heat Transfer Dynamics of Inorganic Mesoporous-Silica Coated GNRs. Mesoporous-silica-coated GNRs have been considered as a novel high surface area biocompatible platform for drug delivery.[3,4,29] It is important to evaluate the effect of the coating on the heat transfer process as well as the effective length of the local heating. From the previous section, we know that the smallest region of localized heat extends about 30 nm from the CTAB capped GNRs, which is achieved with a 1 ps excitation pulse. Stretching the excitation pulse to 10 ns in duration but keeping the same energy will result in the localization of the heat to a region of about 100 nm from the GNRs, and the temperature rise is very small (Figure S4). Thus, we believe the effective length of local heating should fall into this range when using pulsed excitation. We, therefore, prepared two porous-sillica coated GNRs samples with a silica thickness of about 30 nm (here called thin coated) and 90 nm (thick coated) to evaluate the effect of this inorganic coating on the heat transfer dynamics.

In this TRIR experiment, there are two local water environments that contribute to the spectra of the thin-coated GNR samples: water inside the silica shell and water surrounding the shell. To provide the temperature dependence of the water spectra in these two regions, the elevated temperature steady-state IR measurement was performed for the thin film (Figure 2D) and the colloid (Figure S1E) of thick silica coated GNRs. Both measurements show a linear dependence of the water spectral features to temperature changes; thus, the TRIR spectra can be used to monitor the heat transfer dynamics of the thin as well as the thick silica coated samples. Both samples have very similar TRIR spectral features. Figure 3E shows representative spectra of the thin-coated GNR sample. These spectra closely resemble the difference spectra at elevated steady-state temperatures in Figures 2D and S1E, indicating the heat transfer. Similar to the case of CTAB capped GNRs, the positive ΔOD signals in all silica coating samples have the fast decay time constants of few picoseconds, then maintain an unnoticeable change of large positive ΔOD values up to 30 ps. This fast decay does not affect the spectra of heat transfer dynamics.

Figure 3F,G show slower heat transfer dynamics of silica-coated samples than those of the surfactant-capped GNR sample. The thin-coated sample has comparably sized GNR cores to those of the surfactant-capped GNRs; thus, the slower heat transfer must arise due to the silica shell. In comparing samples with thin and thick coatings, the latter has larger sized GNR cores, and a smaller surface-area-to-volume ratio, such that heat transfer would be expected to be slower. The opposite experimental result indicates that the silica clearly affects the heat transfer dynamics. The thermal conductivity of dried mesoporous silica is about 0.2−0.3 W/mK,[30] comparable to that of the CTAB bilayer (0.2 W/mK) in the surfactant capped GNRs,[11] but about a half that of water (0.6 W/mK). The silica coating is a combination of mesoporous silica and water channels, which adds a poor thermal conductor around the surfactant capped GNRs and explains the slower heat transfer through the entire structure. Overall, the thermal conductivity of the water filled mesoporous silica is between 0.3 and 0.6 W/mK. Similar to other studies,[31,32] our observation demonstrates that the medium surrounding the particles, not necessarily just at the interface, also affects the heat transfer. Previous transient absorption spectroscopic studies show the opposite result, with a mesoporous silica coating on spherical gold NPs causing faster heat transfer.[31] The explanation given in that study was that porous silica has a higher thermal conductivity than water. However, later careful measurements on various porous silica thin films with nanoscale thickness show they actually have lower thermal conductivity.[30] Our result is consistent with this latter observation. The presence of the silica shell causes less water to surround the GNR, resulting in a reduction in the heat transfer efficiency. Additionally, the water filling disordered silica channels forms a large interfacial area covering the silica which also reduces the heat transfer efficiency.

On the basis of the discussion so far, one might at first expect a GNR with a thick silica coating to exhibit a longer heat transfer time. However, the experiment shows the opposite trend. A careful look at the shell thickness and the heat diffusion length in each sample provides a reasonable explanation for this observation. For the GNRs with thick coatings, the heat transfer time constant is about 1.2 times longer than that of the bare GNRs, such that we estimate the thermal diffusivity of the shell to be about 1.2 times smaller than that of water. With this estimate, at 2 ns delay, the heat is still diffusing inside the silica with a distance of 31 nm from the GNRs. In GNRs with thick coatings (84−91 nm thickness, Table S1), heat transfers efficiently in the water filled disordered channels inside the silica. In contrast, GNRs with thin coatings have a silica shell thickness of 28−35 nm (Table S1), a comparable value to the above calculated heat diffusion length, thus the heat still diffuses further from the shell through the surfactant surrounding the silica[21] after 2 ns delay and later to the surrounding water. The surfactants block the water channel at the border of the shell, preventing efficient heat transfer from the shell to the outside water, thus causing longer heat transfer times in the thin coated sample (illustrated in Figure 4). Another piece of evidence supporting the heat transfer further out from the silica shell to the surrounding water in the GNRs with thin coatings is the more negative ΔOD at long delay times (comparing kinetic trace in Figure 3F to that in Figure 3G), indicating the strong contribution of the spectra of water outside the silica shell. Though this explanation is supported by the experimental observations, we cannot eliminate the possibility that different porous densities of the silica shells in the thin- and thick-coated GNRs lead to the differences in heat transfer dynamics.

Overall, we showed that the heat transfer dynamics in the mesoporous-silica coated GNRs are slower than those of the CTAB capped GNRs. In the case of GNRs coated with a silica shell of about 30 nm thickness, approximately the smallest region of effective local heating, the heat transfer time is about

DOI: 10.1021/acsnano.5b06623
ACS Nano 2016, 10, 2144−2151

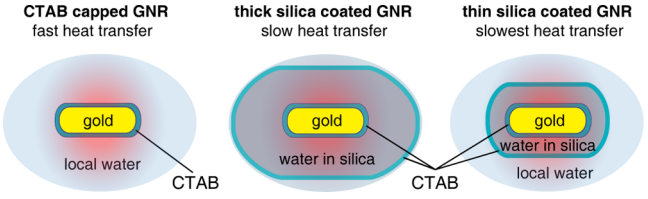

Figure 4. Scheme explaining the heat transfer dynamics in three samples. The thick silica coated GNR has slower heat transfer than the CTAB capped GNR due to the low thermal conductivity of the mesoporous silica in comparison to that of water. Heat still diffuse efficiently in the water channels inside the silica shell. The thin coated GNR has slowest heat transfer because the heat transfer is not efficient through the second layer of CTAB surrounding the silica shell.

600 ps because the heat still partially diffuses further from the silica shell to the water through the thermal resistant CTAB at the silica shell–water interface. CTAB has the highest thermal resistance compared to all of the other materials in the system of silica coated GNRs in water; thus, it retards the efficient heat transfer of the entire system. In the case of very thick coated samples, about 90 nm, the heat transfer time is about 400 ps due to efficient heat diffusion just inside the silica shell. We believe these two samples set the range of heat transfer time and length which will be very useful for the design of an appropriate shell thickness in photothermal applications of porous silica coated NPs.

Formation of a Transient Nanobubble. In the 20 mW experiment, the kinetic trace in the 2140–2180 cm^{-1} region reaches the strongest negative ΔOD at *ca.* 750 ps before recovering to a stable value after 2 ns (Figure 3D). From the previous section, we know that the heat transfer is almost complete and the temperature of the particles and of the local environment is not high at this delay time. The kinetic trace at 2 ns in the 20 mW experiment also obeys a linear relationship between the ΔOD at 2 ns and the excitation power (R^2 = 0.99) in other experiments, indicating that we are detecting total heat dissipation. Thus, the temperature of the local solvent at this long delay time must be below the boiling point of the solution. However, we assign the unusually strong negative ΔOD below the flat trace in the 20 mW experiment to the formation of a transient nanobubble around the particle, formed from surrounding water reaching very high temperatures. The transient bubbles must transmit in this IR region more strongly than the liquid solution, resulting in a strong negative ΔOD. The kinetic trace in the 1980–2000 cm^{-1} region, however, shows non-noticeable ΔOD at this same time scale, indicating that the transient bubbles do not transmit equally among all IR frequencies. This variant behavior of TRIR spectra at the low and high energy regions indicates that the bubbles do not simply exist in the form of water vapor (100 °C, 1 atm); otherwise, the spectra would have similar ΔOD at both energy regions. This spectral behavior also indicates that the change of the refractive index (due to temperature changes) and thus the distortion of the probe beam do not significantly affect the measurement; otherwise, we would see an entirely positive or negative ΔOD (but not both) at this long delay time.[17] Since the 2150 cm^{-1} region is assigned to the combination band of the H–O–H bending and libration vibrations, the strong transmission of this region suggests a decreased population of the libration vibration, due to the breaking of the hydrogen bond network at high temperature.

To estimate the time scale on which the bubbles are formed, we extrapolated the flat kinetic trace at 2.5 ns delay to the earlier delay times and estimated the longest delay time for the bubble formation to be about 300 ps (Figure 3D, black curve). If we adopt the upper limit heat transfer time constant to be about 300 ps in this 20 mW experiment, 1/e of heat has already been transferred to the water at 300 ps delay, giving an estimated temperature of the GNRs of 490 °C; thus, the estimated temperature of the nanobubble is also about this value. In fact, the bubble nucleation in a nanosize region is expected to happen at several hundred degrees above the boiling point (100 °C) of water because of the high curvature and surface tension of the nanosized bubble. This superheating temperature is well-known *via* the classical nucleation theory using the Young–Laplace equation and from other experimental observations.[33−35] The descent of the kinetic trace after the bubble starts forming suggests that the bubble continues growing and that the heat probably continues to transfer from GNRs to the surrounding. The recovery of the kinetic trace after 750 ps indicates that the bubbles collapse slowly due to heat dissipation to the bulk. After 2 ns delay, the bubble has completely vanished. For the two silica coated samples, no bubble formation is observed, as we might expect given that the confined space of the mesopores prevents bubble formation.

It is important to notice that at higher fluence, the excitation pulse causes the shape of the GNRs to transform.[9,36] At 8 mW, a small fraction of GNRs transform to some ill-defined shape. At 20 mW, there are more spherical shaped particles by the end of the experiment (Figure S2), resulting in a change the surface area of the particles. This transformation could happen on the order of hundreds of picoseconds,[36] affecting the heat transfer dynamics. Spherical shaped particles with the same volume to that of GNRs would have smaller surface area-to-volume ratio, and heat transfer would thus be expected to occur more slowly. However, heat transfer still happens fastest in this 20 mW excitation experiment, probably due to the very large temperature rise or the desorption of the capping ligand. On the other hand, the silica coated GNR sample has minor change in shape and in the plasmon absorption (Figure S3). The silica shell acts like a mold to preserve the rod-shape of the core gold particles, even if the core is melted. The enhanced thermal stability of the silica-coated GNR was also observed in a thinner silica-coated GNR (6 nm thick) in another study.[37] This thermal stability allows the silica-coated GNR platform to achieve high local temperature without deformation of their shape or shifting of their SPR absorption.

CONCLUSIONS

We have presented an information-rich spectroscopic approach in which we have probed the IR spectrum of water to study heat transfer dynamics from GNRs to the local aqueous solvent environment. We systematically studied the effect of the organic CTAB capping and inorganic mesoporous-silica coatings of different thicknesses on the heat transfer dynamics. This information will help future researchers optimize and more fully utilize NPs for their numerous and varied applications. We demonstrated that probing the local solvent surrounding the NPs is crucial to understanding the exchange dynamics between the nanomaterial and the environment, especially at the interfaces in the nanoscale region. The advantage of ultrafast spectroscopy is that it instantaneously captures the local heat transfer dynamics prior to equilibration of the solution, such that the observed dynamics are assigned to

DOI: 10.1021/acsnano.5b06623
ACS Nano 2016, 10, 2144–2151

the local environment surrounding the particles. TRIR spectroscopy offers rich structural information about the local environment and carries the potential for future studies on the mechanism of plasmon-mediated chemical reactions and processes.

MATERIAL AND METHOD

In the TRIR spectroscopic experiment, the NPs are excited by 1 ps, 800 nm pulses. The photoexcited electrons relax through the electron thermalization process in few hundred femtoseconds,[38] which is not covered in this study. On the picosecond time scale, the heat transfer and electron ejection from the NPs modifies the IR absorption of the local aqueous solvent, which can be probed by 100 fs mid-IR (~5 μm) pulses with picosecond resolution. In all of the studies, NPs were prepared to have an SPR absorption at ~800 nm *via* the seed growth method.[39] To prepare the sample for the IR and TRIR measurements, the as-synthesized samples were washed with excess water to minimize the effect of small amount of other precursors used in synthesis on our observations on water. Details of synthesis, characterizations, the spectroscopic setup, and calculation of temperature rise are described in the Supporting Information.

ASSOCIATED CONTENT

Supporting Information

The Supporting Information is available free of charge on the ACS Publications website at DOI: 10.1021/acsnano.5b06623.

Additional experimental data (PDF)

AUTHOR INFORMATION

Corresponding Authors

*E-mail: cbharris@berkeley.edu.
*E-mail: weller@chemie.uni-hamburg.de.
*E-mail: alivis@berkeley.edu.

Notes

The authors declare no competing financial interest.

ACKNOWLEDGMENTS

This work is supported by the Physical Chemistry of Inorganic Nanostructures Program, KC3103, Office of Basic Energy Sciences of the United States Department of Energy under Contract DE-AC02-05CH11232 (A.P.A.), NSF Grant CHE-1213135 (C.B.H.), German Federal Cluster of Excellence "The Hamburg Centre for Ultrafast Imaging" (H.W.).

REFERENCES

(1) Huang, X.; El-Sayed, I. H.; Qian, W.; El-Sayed, M. A. Cancer Cell Imaging and Photothermal Therapy in the Near-Infrared Region by Using Gold Nanorods. *J. Am. Chem. Soc.* **2006**, *128*, 2115−2120.

(2) Qin, Z.; Bischof, J. C. Thermophysical and Biological Responses of Gold Nanoparticle Laser Heating. *Chem. Soc. Rev.* **2012**, *41*, 1191−1217.

(3) Skirtach, A. G.; Muñoz Javier, A.; Kreft, O.; Köhler, K.; Piera Alberola, A.; Möhwald, H.; Parak, W. J.; Sukhorukov, G. B. Laser-Induced Release of Encapsulated Materials inside Living Cells. *Angew. Chem., Int. Ed.* **2006**, *45*, 4612−4617.

(4) Biju, V. Chemical Modifications and Bioconjugate Reactions of Nanomaterials for Sensing, Imaging, Drug Delivery and Therapy. *Chem. Soc. Rev.* **2014**, *43*, 744−764.

(5) Neumann, O.; Urban, A. S.; Day, J.; Lal, S.; Nordlander, P.; Halas, N. J. Solar Vapor Generation Enabled by Nanoparticles. *ACS Nano* **2013**, *7*, 42−49.

(6) Neumann, O.; Feronti, C.; Neumann, A. D.; Dong, A.; Schell, K.; Lu, B.; Kim, E.; Quinn, M.; Thompson, S.; Grady, N.; Nordlander, P.; Oden, M.; Halas, N. J. Compact Solar Autoclave Based on Steam Generation Using Broadband Light-harvesting Nanoparticles. *Proc. Natl. Acad. Sci. U. S. A.* **2013**, *110*, 11677−11681.

(7) Linic, S.; Aslam, U.; Boerigter, C.; Morabito, M. Photochemical Transformations on Plasmonic Metal Nanoparticles. *Nat. Mater.* **2015**, *14*, 567−576.

(8) Brongersma, M. L.; Halas, N. J.; Nordlander, P. Plasmon-induced Hot Carrier Science and Technology. *Nat. Nanotechnol.* **2015**, *10*, 25−34.

(9) Link, S.; El-Sayed, M. A. Shape and Size Dependence of Radiative, Non-radiative and Photothermal Properties of Gold Nanocrystals. *Int. Rev. Phys. Chem.* **2000**, *19*, 409−453.

(10) Qiu, J.; Wei, W. D. Surface Plasmon-Mediated Photothermal Chemistry. *J. Phys. Chem. C* **2014**, *118*, 20735.

(11) Huang, J.; Park, J.; Wang, W.; Murphy, C. J.; Cahill, D. G. Ultrafast Thermal Analysis of Surface Functionalized Gold Nanorods in Aqueous Solution. *ACS Nano* **2013**, *7*, 589−597.

(12) Hu, M.; Hartland, G. V. Heat Dissipation for Au Particles in Aqueous Solution: Relaxation Time *versus* Size. *J. Phys. Chem. B* **2002**, *106*, 7029−7033.

(13) Hartland, G. V. Optical Studies of Dynamics in Noble Metal Nanostructures. *Chem. Rev.* **2011**, *111*, 3858−3887.

(14) Schmidt, A. J.; Alper, J. D.; Chiesa, M.; Chen, G.; Das, S. K.; Hamad-Schifferli, K. Probing the Gold Nanorod−Ligand−Solvent Interface by Plasmonic Absorption and Thermal Decay. *J. Phys. Chem. C* **2008**, *112*, 13320−13323.

(15) Kreibig, U. Anomalous Frequency And Temperature Dependence of The Optical Absorption of Small Gold Particles. *J. Phys. Colloq.* **1977**, *38*, C2−97−C2−103.

(16) Link, S.; El-Sayed, M. A. Size and Temperature Dependence of the Plasmon Absorption of Colloidal Gold Nanoparticles. *J. Phys. Chem. B* **1999**, *103*, 4212−4217.

(17) Nguyen, S. C.; Lomont, J. P.; Caplins, B. W.; Harris, C. B. Studying the Dynamics of Photochemical Reactions *via* Ultrafast Time-Resolved Infrared Spectroscopy of the Local Solvent. *J. Phys. Chem. Lett.* **2014**, *5*, 2974−2978.

(18) Pal, S.; Balasubramanian, S.; Bagchi, B. Dynamics of Bound and Free Water in an Aqueous Micellar Solution: Analysis of the Lifetime and Vibrational Frequencies of Hydrogen Bonds at a Complex Interface. *Phys. Rev. E: Stat. Phys., Plasmas, Fluids, Relat. Interdiscip. Top.* **2003**, *67*, 061502.

(19) Piletic, I. R.; Moilanen, D. E.; Spry, D. B.; Levinger, N. E.; Fayer, M. D. Testing the Core/Shell Model of Nanoconfined Water in Reverse Micelles Using Linear and Nonlinear IR Spectroscopy. *J. Phys. Chem. A* **2006**, *110*, 4985−4999.

(20) Lian, T.; Locke, B.; Kholodenko, Y.; Hochstrasser, R. M. Energy Flow from Solute to Solvent Probed by Femtosecond IR Spectroscopy: Malachite Green and Heme Protein Solutions. *J. Phys. Chem.* **1994**, *98*, 11648−11656.

(21) Gorelikov, I.; Matsuura, N. Single-Step Coating of Mesoporous Silica on Cetyltrimethyl Ammonium Bromide-Capped Nanoparticles. *Nano Lett.* **2008**, *8*, 369−373.

(22) Sulpizi, M.; Gaigeot, M.-P.; Sprik, M. The Silica−Water Interface: How the Silanols Determine the Surface Acidity and Modulate the Water Properties. *J. Chem. Theory Comput.* **2012**, *8*, 1037−1047.

(23) Anderson, N. A.; Hang, K.; Asbury, J. B.; Lian, T. Ultrafast Mid-IR Detection of the Direct Precursor to the Presolvated Electron following Electron Ejection from Ferrocyanide. *Chem. Phys. Lett.* **2000**, *329*, 386−392.

(24) Laenen, R.; Roth, T.; Laubereau, A. Novel Precursors of Solvated Electrons in Water: Evidence for a Charge Transfer Process. *Phys. Rev. Lett.* **2000**, *85*, 50−53.

(25) Kamat, P. V.; Flumiani, M.; Hartland, G. V. Picosecond Dynamics of Silver Nanoclusters. Photoejection of Electrons and Fragmentation. *J. Phys. Chem. B* **1998**, *102*, 3123−3128.

(26) Cooper, F. Heat Transfer from a Sphere to an Infinite Medium. *Int. J. Heat Mass Transfer* **1977**, *20*, 991−993.

DOI: 10.1021/acsnano.5b06623
ACS Nano 2016, 10, 2144−2151

(27) Haynes, W. M., Ed.; *CRC Handbook of Chemistry and Physics*, 95th ed. (Internet Version 2015); CRC Press/Taylor and Francis: Boca Raton, FL, 2015.
(28) Landau, L.D.; Lifshitz, E. M. *Fluid Mechanics*, 2nd ed; Pergamon Press: New York, 1987; p 192.
(29) Zhang, Z.; Wang, L.; Wang, J.; Jiang, X.; Li, X.; Hu, Z.; Ji, Y.; Wu, X.; Chen, C. Mesoporous Silica-Coated Gold Nanorods as a Light-Mediated Multifunctional Theranostic Platform for Cancer Treatment. *Adv. Mater.* **2012**, *24*, 1418−1423.
(30) Coquil, T.; Richman, E. K.; Hutchinson, N. J.; Tolbert, S. H.; Pilon, L. Thermal Conductivity of Cubic and Hexagonal Mesoporous Silica Thin Films. *J. Appl. Phys.* **2009**, *106*, 034910.
(31) Hu, M.; Wang, X.; Hartland, G. V.; Salgueiriño-Maceira, V.; Liz-Marzán, L. M. Heat Dissipation in Gold−silica Core-shell Nanoparticles. *Chem. Phys. Lett.* **2003**, *372*, 767−772.
(32) Ge, Z.; Kang, Y.; Taton, T. A.; Braun, P. V.; Cahill, D. G. Thermal Transport in Au-Core Polymer-Shell Nanoparticles. *Nano Lett.* **2005**, *5*, 531−535.
(33) Witharana, S.; Phillips, B.; Strobel, S.; Kim, H. D.; McKrell, T.; Chang, J.-B.; Buongiorno, J.; Berggren, K. K.; Chen, L.; Ding, Y. Bubble Nucleation on Nano- to Micro-size Cavities and Posts: an Experimental Validation of Classical Theory. *J. Appl. Phys.* **2012**, *112*, 064904.
(34) Baral, S.; Green, A. J.; Livshits, M. Y.; Govorov, A. O.; Richardson, H. H. Comparison of Vapor Formation of Water at the Solid/Water Interface to Colloidal Solutions Using Optically Excited Gold Nanostructures. *ACS Nano* **2014**, *8*, 1439−1448.
(35) Hou, L.; Mustafa, Y.; Nico, R. V.; Michel, O. Explosive Formation and Dynamics of Vapor Nanobubbles around a Continuously Heated Gold Nanosphere. *New J. Phys.* **2015**, *17*, 013050.
(36) Petrova, H.; Perez Juste, J.; Pastoriza-Santos, I.; Hartland, G. V.; Liz-Marzan, L. M.; Mulvaney, P. On the Temperature Stability of Gold Nanorods: Comparison between Thermal and Ultrafast Laser-induced Heating. *Phys. Chem. Chem. Phys.* **2006**, *8*, 814−821.
(37) Chen, Y.-S.; Frey, W.; Kim, S.; Homan, K.; Kruizinga, P.; Sokolov, K.; Emelianov, S. Enhanced Thermal Stability of Silica-coated Gold Nanorods for Photoacoustic Imaging and Image-guided Therapy. *Opt. Express* **2010**, *18*, 8867−8878.
(38) Link, S.; El-Sayed, M. A. Optical Properties and Ultrafast Dynamics of Metallic Nanocrystals. *Annu. Rev. Phys. Chem.* **2003**, *54*, 331−366.
(39) Ye, X.; Zheng, C.; Chen, J.; Gao, Y.; Murray, C. B. Using Binary Surfactant Mixtures To Simultaneously Improve the Dimensional Tunability and Monodispersity in the Seeded Growth of Gold Nanorods. *Nano Lett.* **2013**, *13*, 765−771.

DOI: 10.1021/acsnano.5b06623
ACS Nano 2016, 10, 2144−2151